Published online 5 May 2021

Nucleic Acids Research, 2021, Vol. 49, No. 9 ***5369–5381***
doi: 10.1093/nar/gkab316

PIN and CCCH Zn-finger domains coordinate RNA targeting in ZC3H12 family endoribonucleases

Ankur Garg [1,2,*], Yvette Roske[1], Shinnosuke Yamada[3], Takuya Uehata[3], Osamu Takeuchi [3] and Udo Heinemann [1,2,*]

[1]Macromolecular Structure and Interaction, Max-Delbrück Center for Molecular Medicine in the Helmholtz Association, Robert-Rössle-Str. 10, 13125 Berlin, Germany, [2]Institute for Chemistry and Biochemistry, Freie Universität Berlin, Takustr. 6, 14195 Berlin, Germany and [3]Department of Medical Chemistry, Graduate School of Medicine, Kyoto University, Kyoto, Japan

Received July 03, 2020; Revised April 12, 2021; Editorial Decision April 14, 2021; Accepted April 15, 2021

ABSTRACT

The CCCH-type zinc finger (ZnF) containing ZC3H12 ribonucleases are crucial in post-transcriptional immune homoeostasis with ZC3H12A being the only structurally studied member of the family. In this study, we present a structural-biochemical characterization of ZC3H12C, which is linked with chronic immune disorders like psoriasis. We established that the RNA substrate is cooperatively recognized by the PIN and ZnF domains of ZC3H12C and analyzed the crystal structure of ZC3H12C bound to a single-stranded RNA substrate. The RNA engages in hydrogen-bonded contacts and stacking interactions with the PIN and ZnF domains simultaneously. The ZC3H12 ZnF shows unprecedented structural features not previously observed in any member of the CCCH-ZnF family and utilizes stacking interactions via a unique combination of spatially conserved aromatic residues to align the target transcript in a bent conformation onto the ZnF scaffold. Further comparative structural analysis of ZC3H12 CCCH-ZnF suggests that a trinucleotide sequence is recognized by ZC3H12 ZnF in target RNA. Our work not only describes the initial structure-biochemical study on ZC3H12C, but also provides the first molecular insight into RNA recognition by a ZC3H12 family member. Finally, our work points to an evolutionary code for RNA recognition adopted by CCCH-type ZnF proteins.

INTRODUCTION

Inflammatory and immune responses are tightly controlled at post-transcriptional levels by RNA binding proteins (RBPs) to prevent an autoimmune condition caused by overexpression of immune factors including cytokines (1). Among more than one thousand identified RBPs in mammals (2), a majority of immune regulatory RBPs are known to interact with *cis*-elements present in the 3′ untranslated regions (3′ UTRs) of mRNAs and modulate the half-life of their target transcripts (3–5). Regulatory RNase (Regnase)/ZC3H12/MCPIP family proteins are unique CCCH-type zinc finger (ZnF) containing ribonucleases, which are crucial in maintaining immune homeostasis. All four ZC3H12 family members have a conserved PilT N-terminus (PIN) RNase domain, with ZC3H12A/Regnase-1 and ZC3H12C/Regnase-3 being highly upregulated upon lipopolysaccharide (LPS) mediated Toll-like receptor (TLR) activation in macrophages (6–8), suggesting their involvement in innate immune responses.

ZC3H12C/Regnase-3/MCPIP-3 is the third and largest member of the ZC3H12 family, and its physiological functions have been associated with prevention of autoimmune conditions like psoriasis in European and Pakistani populations via regulating tumor necrosis factor (TNF)-α and T_H cell activation (9,10). ZC3H12C deficient mice developed hypertrophic lymph nodes and a higher proportion of immature B-cells and innate immune cells via IFN signaling in myeloid cells (11). ZC3H12C has also been involved in controling pro-inflammatory cytokines by suppressing NF-κB activation in human umbilical vein endothelial cells (HUVECs) (12). Within the whole family, ZC3H12A has been the best-studied member so far, and mice lacking ZC3H12A show severe autoimmune inflammatory disease with augmented levels of serum antibodies and plasma cells (8). ZC3H12A not only regulates cytokines including IL-6, IL-

*To whom correspondence should be addressed. Tel: +49 30 9406 3420; Fax: +49 30 9406 2548; Email: heinemann@mdc-berlin.de
Correspondence may also be addressed to Ankur Garg. Email: garg@cshl.edu
Present address: Ankur Garg, W.M. Keck Structural Biology Laboratory, Cold Spring Harbor Laboratory, 1 Bungtown Road, Cold Spring Harbor, NY 11724, USA.

12p40, IL-1β and IL-8 (8,13,14), but also Nfkbiz, Nfkbid, Ptgs2, Id1, Cxcl1–3 and ZC3H12A (15,16) by directly catalyzing degradation of their transcripts. A mechanistic study showed that a highly conserved stem-loop structure in its mRNA 3′ UTR is essential (15), which is cleaved at the single-stranded Py–Pu–Py loop region (17) by the PIN domain of ZC3H12A.

CCCH-type ZnF containing proteins are attributed with regulating diverse physiological functions with several of them involved in immune response regulation (18) by recognizing specific single-stranded (ss) RNA sequences. The tris-tetraproline (TTP) and Nab2 proteins regulate inflammatory cytokine expression and mRNA polyadenylation by binding with AU-rich elements (AREs) such as rAUUUA (19) and poly-A sequences (20,21), respectively, via their multiple CCCH ZnFs. Another CCCH ZnF containing protein, Roquin, downregulates cytokine expression by binding with a single-stranded Py–Pu–Py tri-loop in a constitutive decay element (CDE) in cytokine mRNA via its ROQ domain (22–24). The ZC3H12 CCCH-ZnF has a conserved $C^1X_5C^2X_5C^3X_3H$ consensus sequence, and despite its vital role in immune response regulation, structural insights on CCCH-type ZnF mediated RNA recognition still remain elusive. In addition, structural aspects of the coordinated targeting of novel RNA (25) stem–loop structures by RNases with PIN and ZnF domain (ZFD) are poorly explored.

To obtain much needed functional and mechanistic insight into ZC3H12 protein-mediated negative regulation of immune responses, we undertook a structural and biochemical analysis of Regnase-3/ZC3H12C. We determined multiple crystal structures of the mouse ZC3H12C PIN domain and ZC3H12C PIN-ZFD bound to an RNA heptamer, revealing unprecedented detail in RNA recognition by both domains for the first time. Our biochemical experiments confirm that ZC3H12C is an active RNase, which requires its N- and C-motif for regulated *in vivo* RNase activity against the target RNA substrate. Mutational analysis reveals unique structural features of the ZC3H12 CCCH-ZnF in ssRNA recognition and, together with a small number of studied CCCH-ZnFs, provides a basis to predict the RNA binding pattern of other CCCH-ZnFs, for which experimental structures are not yet available.

MATERIALS AND METHODS

Cloning, expression and protein purification

Different cDNAs encoding the *Mus musculus* (*Mm*) ZC3H12C full-length (FL), PIN/ribonuclease (RNase) domain and ZFD were subcloned into the pQLinkH (26) or N-flag_pcDNA vector. Catalytic mutants were generated using the QuikChange Site-Directed Mutagenesis Kit (Stratagene) according to the manufacturer's protocol. Protein-coding genes were expressed with a cleavable N-terminal 7× His-tag in *Escherichia coli* Rosetta 2 (DE3) cells (Novagen), which were grown up to an OD_{600} of ∼1.0 at 37°C in Terrific Broth (TB) medium. Protein expression was then induced at 18°C for 16 h by adding 0.5 mM IPTG. The purification procedure included Ni-affinity chromatography on a 5 ml HisTrap HP column (GE Healthcare), cleavage of the 7× His-tag using tobacco etch virus (TEV) protease, a second Ni-affinity chromatography, followed by size-exclusion chromatography (SEC) on a Superdex 75 column (16/60 or 26/60 column, GE Healthcare). All purification steps were performed at 4°C, and for constructs containing the ZFD, all purification buffers were supplemented with 20 μM $ZnSO_4$.

Escherichia coli cells overexpressing the protein were resuspended in lysis buffer (1× PBS pH 7.4, 0.5 M NaCl, 5% (v/v) glycerol, 2.5 mM β-mercaptoethanol (βMe) supplemented with 1 μg/ml DNase I (Roche), 1 U/ml Benzonase (Merck) and one tablet of EDTA-free Complete Protease Inhibitor (Roche) followed by cell disruption using a microfluidizer (Microfluidics). The soluble fraction of the lysate was separated by centrifugation at 45 000 *g* for 1 h, filter-sterilized through a 0.2 μm pore-size filter and applied on a 5 ml HisTrap HP column. The column was equilibrated with 5 column volumes (CVs) of buffer-1 (25 mM HEPES pH 7.5, 200 mM NaCl, 10 mM imidazole, 2.5 mM βMe) and washed with 10 CVs of buffer-2 (25 mM HEPES pH 7.5, 500 mM NaCl, 25 mM imidazole, 2.5 mM βMe) followed by protein elution with 5–10 CVs of buffer-3 (25 mM HEPES pH 7.5, 200 mM NaCl, 250 mM imidazole, 2.5 mM βMe). The eluate was dialyzed overnight against buffer-1 supplemented with 5% glycerol, 1 mM $MgCl_2$ together with 1 mg 6× His-tagged TEV protease per 10 mg protein, and reapplied on a 5 ml HisTrap HP column to remove the cleaved tag and 6× His-TEV protease. The collected flow-through was concentrated and applied to the SEC using buffer-4 (25 mM HEPES pH 7.5, 150 mM NaCl, 1 mM DTT, 1 mM $MgCl_2$), and the peak fractions were pooled, concentrated to ∼10 mg/ml and stored at –80°C after flash-freezing in liquid nitrogen.

Protein crystallization

Purified *Mm*ZC3H12C proteins were crystallized at 20°C, while the *Mm*ZC3H12C-RNA complex was crystallized at 4°C using the sitting-drop vapor-diffusion method by mixing equal volumes of protein or protein-oligonucleotide complex solution and the reservoir buffer in a drop volume of 400 nl. Crystals of N-$PIN^{(177–425)}$ were obtained by mixing 10.2 mg/ml protein (25 mM HEPES pH 7.5, 150 mM NaCl, 1 mM DTT) with 0.2 M LiCl, 50 mM $MgSO_4$ and 8% PEG 8000 as reservoir solution. PIN-$Zf^{(260–458)}$ was crystallized by mixing 10 mg/ml protein (25 mM HEPES pH 7.5, 150 mM NaCl, 1 mM DTT, 1 mM $MgCl_2$, 20 μM $ZnSO_4$) with 0.2 M LiCl, 20% PEG 6000 and 0.1 M HEPES pH 7.0 as reservoir solution, and single crystals for the $PIN^{(260–425)}$(D271N) mutant were obtained by mixing 10 mg/ml protein (25 mM HEPES pH 7.5, 150 mM NaCl, 1 mM DTT, 1 mM $MgCl_2$) with 0.2 M KSCN, 20% PEG 3350 and 0.1 M Bis–Tris propane pH 6.5 as reservoir buffer.

The RNA oligonucleotide r(UUAUUAU) was obtained from Integrated DNA Technology (IDT) Inc. and the *Mm*ZC3H12C·r(UUAUUAU) complex was crystallized by mixing 0.32 mM of purified PIN-$Zf^{(260–458)}$(D271N) with a 1.5-fold molar excess of the oligonucleotide in 25 mM HEPES pH 7.5, 150 mM NaCl, 1 mM DTT, 1 mM $MgCl_2$, 20 μM $ZnSO_4$. The mixture was incubated for 30 min at 4°C prior to crystallization, which yielded crystals at 4°C

Table 1. Summary of X-ray data and structure refinement statistics for different crystal structures of *Mm*ZC3H12C

	N-PIN (Mg^{2+}) (7ndi)	PIN-Zf (7ndh)	PIN (D271N) (7ndk)	PIN-Zf • r(UUAUUAU) (7ndj)
Beamline	BESSY II 14.1	BESSY II 14.1	BESSY II 14.1	BESSY II 14.1
Wavelength (Å)	0.91841	0.91841	0.91841	0.91841
Space group	$P3_121$	$P4_12_12$	$P2_1$	$P4_1$
Cell dimensions				
a, *b*, *c* (Å)	114.70, 114.70, 257.31	80.33, 80.33, 143.20	38.75, 61.47, 111.62	63.25, 63.25, 114.54
α, β, γ (°)	90, 90, 120	90, 90, 90	90, 90.06, 90	90, 90, 90
Resolution (Å)	48.8–2.88 (3.05–2.88)	44.5–1.94 (2.06–1.94)	38.7–2.34 (2.48–2.34)	42.4- 1.65 (1.75–1.65)
No of reflections	261 252	267 371	48 975	248 907
Unique reflections	45 274	35 486	21 746	53 908
R_{meas} (%)	14.3 (104.1)	7.9 (106.0)	8.7 (105.3)	8.9 (126.9)
$<I/\sigma(I)>$	13.44 (1.81)	20.51 (1.96)	10.19 (1.41)	11.04 (1.27)
$CC_{1/2}$	0.99 (0.72)	0.99 (0.69)	0.99 (0.63)	0.99 (0.75)
Completeness (%)	99.6 (98.1)	99.9 (99.7)	97.0 (96.7)	99.5 (99.3)
Multiplicity	5.77	7.53	2.25	4.6
Refinement				
R_{work}/R_{free}	0.194/0.217	0.172/0.213	0.229/0.275	0.175/0.208
No of atoms				
Protein	5370	2717	5130	2902
Nucleic acid	0	0	0	121
Hetero atoms	19	33	2	35
Solvent atoms	205	260	94	376
RMSD				
Bond lengths (Å)	0.003	0.011	0.008	0.010
Bond angles (°)	0.740	1.251	1.269	0.945
Ramachandran statistics				
Most favored (%)	98.2	97.9	91.5	98.3
Allowed (%)	1.7	2.1	8.2	1.7
Outliers (%)	0.1	0.0	0.3	0.0
Rotamer outlier (%)	0.5	0.0	1.6	0.0

[a]Values in parentheses represent the highest resolution shell.

with reservoir buffer containing 18% PEG 3350 and 0.2 M sodium fluoride pH 6.9 in a 1.5 μl drop volume. All crystals were harvested and cryo-protected using reservoir solution supplemented with 20% ethylene glycol and flash-frozen in liquid nitrogen.

X-ray data collection, structure determination and refinement

X-ray diffraction data were collected on beamline BL14.1 at the BESSY II electron storage ring operated by the Helmholtz–Zentrum Berlin (HZB), Berlin, Germany (27), at a wavelength of 0.9184 Å. Data were processed with XDSAPP (28), and the phase problem was solved by molecular replacement (MR) using Phaser (29) and *Hs*ZC3H12A (PDB id 3v34) (30) as template for N-PIN$^{(177–425)}$, while other datasets were phased using the ZC3H12C N-PIN$^{(177–425)}$ structure as template. After an initial round of automatic model building by Autobuild (31), WinCoot (32) was used for map and model visualization and further model building. The atomic model was further refined using Phenix.Refine or CCP4.Refmac5 (33). For refinement of ZC3H12C apo structures, non-crystallographic symmetry (NCS) restraints were used simultaneously with secondary structure restraints. For the *Mm*ZC3H12C•r(UUAUUAU) complex model, additional TLS restraints were included together with secondary structure restraints. TLS groups were determined using the TLS Motion Determination (TLSMD) webserver (34). All atomic contacts and the geometry of the atomic models were evaluated using the Molprobity server (35,36), and molecular drawings were generated using the PyMOL molecular graphics system (Version 1.7.0.5, Schrodinger, LLC). The APBS tool (37) was used for calculating electrostatic surface potentials. The data collection and refinement statistics for all structures are summarized in Table 1, and resulting structures were deposited in the RCSB PDB.

In vitro RNA degradation assay

The *Mm*IL-6 3′UTR_WT (403 nt), stem-loop mutant (Mutant1), and stem-loop deletion (ΔSL) RNA variants were synthesized by *in vitro* transcription (IVT) using HiScribe T7 High yield RNA synthesis kit (NEB Inc), and the IL-6–3′UTR stem-loop (SL) oligonucleotide (3′UTR nucleotides 86–103) was commercially synthesized (Eurofins). For *in vitro* RNase assays, 200 ng of the re-annealed RNA substrate was incubated with 1 μg of purified protein for 10–20 min in a total volume of 10 μl in buffer-I (20 mM Tris pH 8.0, 100 mM KCl, 1 mM $MgCl_2$, 1 mM DTT, 25 μM $ZnSO_4$, 0.2 U/ml RNasin) and analyzed on 6% denaturing urea-PAGE.

To investigate the Mg^{2+} ion dependency of the RNase activity, RNA degradation was carried out in buffers containing Mg^{2+} (buffer-I) or EDTA (buffer-I with 1 mM EDTA). ZC3H12C proteins were additionally purified in Mg^{2+} deficient buffers and were also used in RNA degradation assays in buffer-II (buffer-I without Mg^{2+}) as well (marked with red minus sign in Figure 1F). After 20 min, the catalytic reactions were stopped by adding 2x RNA loading dye (NEB) and heating the samples at 95°C for 2 min, followed by analysis on 6% urea–PAGE. RNA fragments were stained using SYBR-Gold (Invitrogen) and visualized on a LAS 4000 gel

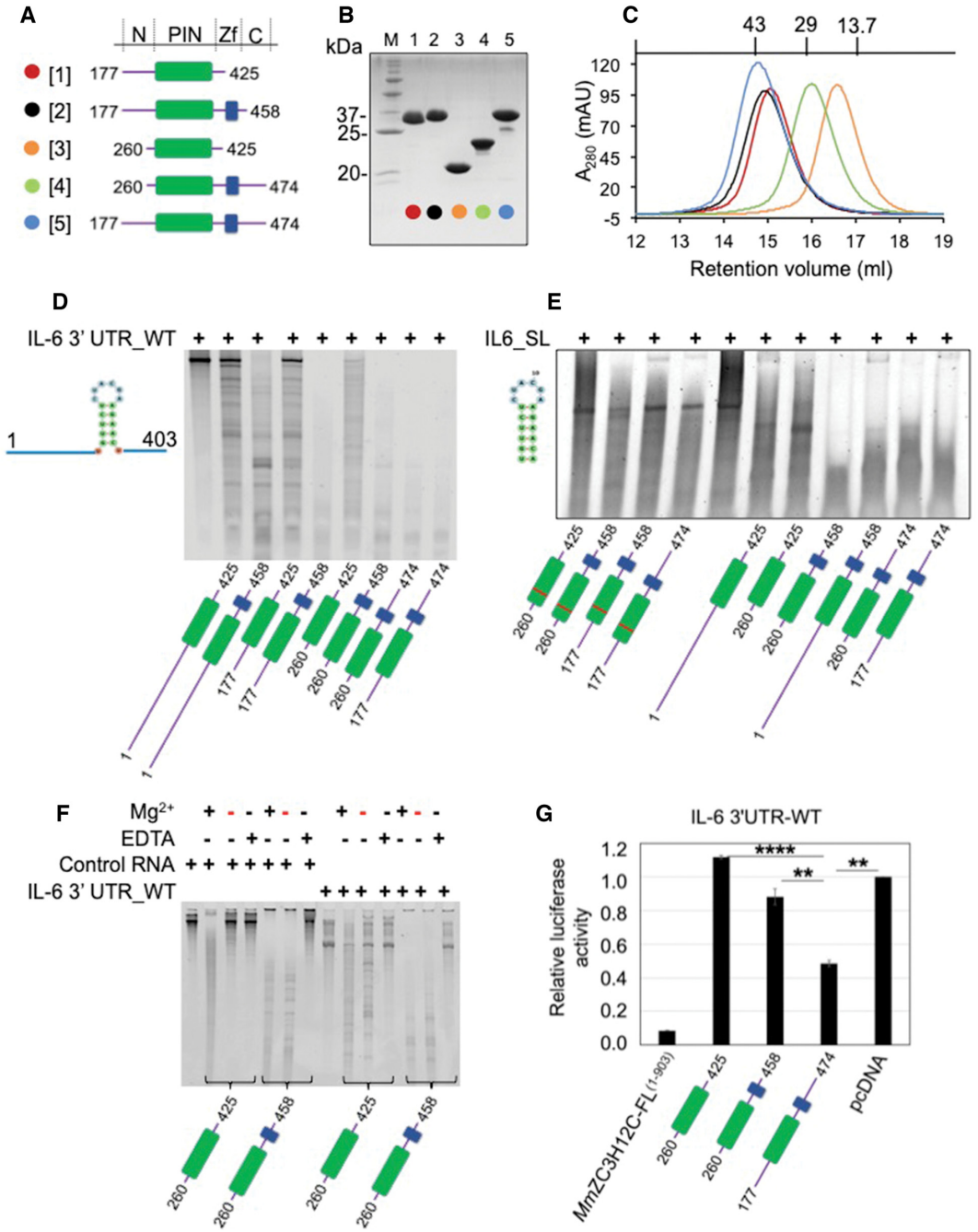

Figure 1. Purification and RNase activity of *Mm*ZC3H12C proteins. (**A**) Domain architecture of designed and purified *Mm*ZC3H12C protein constructs. The constructs primarily harboring the N-motif, PIN domain (green), CCCH ZnF (blue) and C-motif were designed based on the domain and motif annotation as given at the top. A color and number code for each construct is shown on the left. (**B**) A 15% SDS-PAGE showing purified *Mm*ZC3H12C constructs with construct numbers at the top. The pre-stained protein ladder (M) was used as molecular weight marker, with relevant bands labeled with their approximate molecular weight. (**C**) Superdex S75 size exclusion chromatograms (SEC) of the purified proteins demonstrating monomeric state in solution. All chromatograms are color-coded, and molecular weight standards are shown at the top. (**D, E**) Denaturing PAGE analyzing RNase activity of different purified ZC3H12C variants against IL-6 3′UTR RNA oligonucleotide (403 nt) and conserved stem-loop (SL) RNA oligonucleotide (18 nt), respectively. All recombinant proteins displayed high catalytic activity and degraded the substrate RNA into smaller oligonucleotides. The PIN domain (green) exhibits enhanced RNase activity together with the ZFD (blue), suggesting cooperative RNA binding by both PIN and ZFD. The ZC3H12C-D271N mutants (marked with red bar in the PIN domain) exhibit either no *in vitro* RNase activity or a reduced, residual activity in the case of PIN-$Zf^{260–458}$. (**F**) 6% Urea-PAGE demonstrating the dependence on Mg^{2+} ions of the ZC3H12C *in vitro* RNase activity. Both protein fragments catalyzed cleavage of the RNA substrate in presence of Mg^{2+} (in the reaction buffer) but not in presence of EDTA. Proteins purified in buffers without Mg^{2+} (red minus sign) also show RNase activity likely due to Mg^{2+} ions captured in the PIN core during protein expression. The control RNA (firefly luciferase mRNA) is also degraded by ZC3H12C, demonstrating a non-specific RNase activity *in vitro*. (**G**) Luciferase reporter assay demonstrating the activity of *Mm*ZC3H12C against the IL-6 3′UTR. *Mm*ZC3H12C-FL protein (aa 1–903) displays high catalytic activity. The N-PIN-Zf-C (aa 177–474) element of ZC3H12C, but not the PIN (aa 260–425) or PIN-Zf (aa 260–458) constructs degrade the RNA, which implicates the involvement of unstructured N (aa 177–260) or C (aa 458–474) motifs in RNA targeting. The data are presented as mean ± SD ($n = 3$). $^{**}P < 0.01$; $^{****}P < 0.0001$ (two-tailed Student's *t*-test).

documentation system (Fujifilm). *In vitro* transcribed firefly luciferase mRNA was used as control RNA in degradation experiments.

Characterization of ZC3H12 ZFD mutants

RNA degradation efficiency of ZC3H12C Tyr/Ala and Gly/Ala mutants was analyzed by incubating ∼750 ng IL-6 3′UTR_WT with 1 μg of purified protein for 5–15 min in a total 10 μl of 20 mM Tris pH 7.0, 100 mM NaCl, 1 mM $MgCl_2$, 1 mM DTT, 25 μM $ZnSO_4$, 0.2 U/ml RNasin. The reaction was stopped by adding 2× RNA loading dye (Invitrogen), heat-inactivation at 70°C for 5 min, followed by analysis on a 1.2% formaldehyde agarose gel and visualization using a Gel Doc-XR+ system (Bio-Rad).

Luminescence based reporter assay

HEK293T cells were transfected with the luciferase reporter plasmid pGL3 containing the indicated IL-6-3′UTR or ZC3H12A 3′UTR (16), together with the expression plasmids for ZC3H12C variants or empty plasmid as control. 0.8×10^6 cells/well were seeded in a 24-well plate 24 h prior to transfection, and 500 ng of each plasmid was transfected using Lipofectamine-LTX and Plus (Invitrogen) according to the manufacturer's protocol. 25 ng of pRL-(Renilla luciferase)-TK was simultaneously transfected as transfection control. 48 h post transfection, cell were lysed, and luciferase reporter activity was measured using the Dual-luciferase Reporter Assay System (Promega) with a TECAN Infinite M200 luminescence plate reader (Tecan). Data are presented as mean ± SD ($n = 3$).

RESULTS

ZC3H12C is a Mg^{2+} ion dependent ribonuclease

To establish that ZC3H12C is an active RNase, purified proteins (Figure 1A–C) were incubated with different RNA substrates in an *in vitro* RNA degradation assay. Since IL-6 3′UTR is targeted by ZC3H12A, which has a very similar RNase domain structure to ZC3H12C, we used IL-6 3′UTR_WT and the stem-loop (SL) sequence cleaved by ZC3H12A (15) as RNA substrates. IL-6 3′UTR_WT was *in vitro* transcribed, while the 18 nt long IL-6 3′UTR_SL RNA substrate was commercially synthesized. The firefly luciferase mRNA was used as control RNA substrate. All purified ZC3H12C proteins degraded both RNA substrates with different efficiency confirming their RNase activity. Distinctively, ZC3H12C exhibited a ZnF-mediated enhancement in *in vitro* RNase activity, as proteins harboring the ZFD degraded the substrate RNA much more efficiently than proteins harboring only the PIN domain, suggesting involvement of both structured domains of ZC3H12C in RNA targeting (Figure 1D). A D271N mutation of the catalytic residue in the PIN domain exhibited a loss of catalytic activity (Figure 1E).

Since a Mg^{2+} ion was identified bound in the catalytic site in the N-PIN$^{(177–425)}$ crystal structure (see Figure 2A), its role in the ZC3H12C RNase activity was further examined. The IL-6 3′UTR_WT was incubated with ZC3H12C proteins purified in buffers with or without $MgCl_2$. Within 20 min, both ZC3H12C proteins degraded the substrate RNA, with the construct harboring the ZFD showing enhanced RNA degradation. Removal of Mg^{2+} from the reaction by addition of EDTA protected the RNA against degradation, confirming a Mg^{2+} ion dependent RNase activity of ZC3H12C (Figure 1F). Notably, proteins purified in Mg^{2+} deficient buffers (indicated by a red minus sign in the Mg^{2+} row), also exhibited high RNase activity, which most probably resulted from Mg^{2+} ions captured in the PIN domain during protein expression and purification. Interestingly, the control RNA was non-specifically degraded in a Mg^{2+} ion dependent manner, which points to the involvement of either natively unfolded regions of ZC3H12C or of adaptor proteins in mediating the regulation of the RNase activity *in vivo*.

ZC3H12C suppresses IL-6 mRNA 3′UTR upon overexpression

Similar to ZC3H12A (8, 15), ZC3H12C has also been proposed to regulate cytokines by targeting sequences in their mRNA 3′ UTR. Hence, we tested if the IL-6 3′UTR, a confirmed RNA target of ZC3H12A (15), is degraded by *Mm*ZC3H12C in a luciferase reporter assay. The full-length protein, ZC3H12C_FL$^{(1-903)}$, significantly degraded IL-6 3′UTR, as observed by reduction in luciferase activity (Figure 1G). Furthermore, ZC3H12C-PIN$^{(260–425)}$ and ZC3H12C-PIN-Zf$^{(260–458)}$, which displayed high RNase activity towards three different 3′UTR variants *in vitro* (Figure S1A), failed to show any activity towards IL-6 3′UTR_WT in luciferase assays. However, ZC3H12C N-PIN-Zf-C$^{(177–474)}$ harboring sequences N-proximal to the PIN domain and C-proximal to the ZFD, not only degraded the WT 3′UTR (Figure 1G), but also exhibited specificity towards the stem-loop structure (Figure S1B), which was previously shown to be crucial for ZC3H12A mediated degradation (15). ZC3H12C N-PIN-Zf-C$^{(177–474)}$ mediated 3′UTR degradation strongly indicates the involvement of N- and C-motifs in a controlled RNase activity. In ZC3H12A, a similar N-motif close to the RNase domain catalyzes cleavage of target RNA by interacting with the RNA helicase UPF1 (15), and it seems likely that the ZC3H12C N- or C-motifs present similar binding elements to a yet unidentified adaptor protein to regulate the RNase activity.

Overall structure of the ZC3H12C PIN/RNase domain

To investigate the structural basis of the ZC3H12C ribonuclease activity, we crystallized the N-PIN$^{(177–425)}$ and PIN-Zf$^{(260–458)}$ segments of ZC3H12C, as well as a catalytic mutant, PIN$^{(260–425)}$(D271N), (Figure S2A–D) and analyzed their structures (Table 1). The N-PIN crystals belonged to space group $P3_121$ with 4 molecules in one asymmetric unit, while PIN-Zf crystallized in $P4_12_12$ with 2 molecules per asymmetric unit. The N-PIN structure model lacks the N-motif (aa 177–260), for which interpretable electron density is not observed, but aa 261–425 could be unambiguously traced in the electron density. For the PIN-Zf atomic model, clear electron density was observed for the PIN domain (aa 260–428) only, while the ZFD (aa 429–458) was

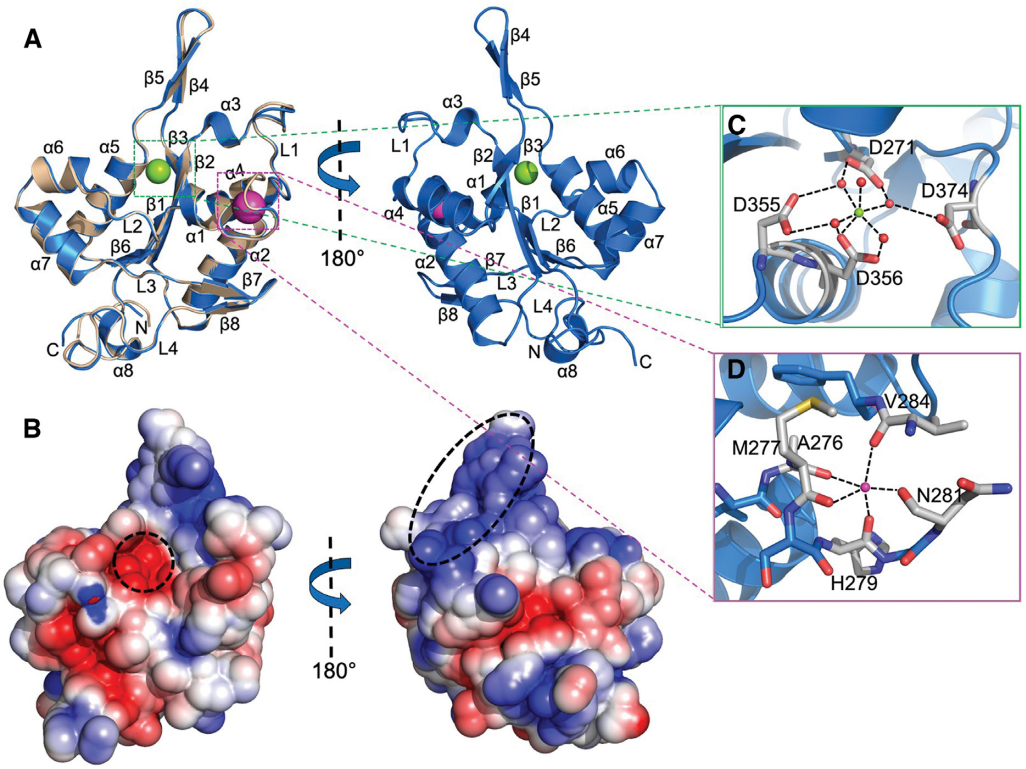

Figure 2. Crystal structures of the *Mm*ZC3H12C PIN/RNase domain. (**A**) Cartoon representation of the *Mm*ZC3H12C N-PIN (blue) structure superimposed onto the PIN-Zf (wheat) structure in front and back orientations. Both structures are virtually identical with a typical Rossmann-like α/β/α sandwich fold. The structure models only show the PIN domains, as electron density for N-motif and ZFD was not observed. A Mg^{2+} ion (green sphere) is trapped in the catalytic site, and a Na^{+} ion (magenta sphere) is bound with the main chain. (**B**) The electrostatic surface potential of PIN shown in two orientations as in the cartoon representation. The PIN domain has a polar surface and exhibits a negatively charged catalytic core and a positively charged region (corresponding to β4/β5) (both highlighted) involved in Mg^{2+} ion and RNA binding. The electrostatic surface potential is displayed in a range from –5 (red) to +5 kT/e (blue). Molecular interactions involving (**C**) the Mg^{2+} and (**D**) the Na^{+} ion with the PIN domain. Mg^{2+} is coordinated between four catalytic aspartate residues (D271, D355, D356, D374) with only one direct contact to D356 and bridging water molecules forming a canonical octahedral geometry, while the Na^{+} ion is stabilized between α1and α2 by five hydrogen bonds with main chain carbonyl oxygens of the residues shown in the figure.

disordered and extended into the solvent region without any traceable electron density. SDS-PAGE analysis of PIN-Zf crystals confirmed that the ZFD was not degraded; evidently, this domain could not be packed in the crystal lattice (data not shown). The crystallized catalytic mutant, PIN (D271N), belonged to space group $P2_1$, with the asymmetric unit accommodating 4 protein molecules, and showed clear electron density for all residues of PIN domain, except for aa 348–350.

The three ZC3H12C RNase domain models are nearly identical with a root-mean-square deviation (RMSD) of 0.20 Å for the matching Cα atoms of N-PIN$^{(177–425)}$ and PIN-Zf$^{(260–458)}$. The PIN domain consists of eight α-helices and eight β-strands, which fold into a butterfly shaped structure. The secondary structure elements are arranged in a typical Rossmann-like α/β/α sandwich fold with a parallel β-sheet (formed by β1, β2, β3 and β6) at the core, surrounded by sets of α-helices on both the sides (α1, α2, α4; and α5, α6, α7) (Figure 2A). Overall, the RNase domain is globular with one antiparallel β-ladder (β4/β5) extending out from the protein surface. A Dali (38) search also suggested that ZC3H12C is a RNase and shares the highest structural similarity with the endoribonuclease ZC3H12A PIN domain (PDB 3v33) (30) with an RMSD of 0.6 Å for 163 aligned Cα atoms, while T5 D15 5′-exonuclease (PDB 1exn) (39) structurally aligns with an RMSD of 3.4 Å for 116 residues.

The electrostatic surface of the ZC3H12C RNase domain is mainly decorated with charged and polar residues with a negatively charged catalytic core (Figure 2B) characterized by four conserved aspartate residues (Asp271, Asp355, Asp356 and Asp374). In the N-PIN$^{(177–425)}$ structure, a Mg^{2+} ion was identified bound in an octahedral geometry at the catalytic core via direct interaction with Asp356 and water-mediated bridges with Asp271, Asp355 and Asp374 (Figure 2C). The ZC3H12A PIN domain (PDB: 3v34) also exhibits a Mg^{2+} ion bound between Asp residues suggesting a similar catalytic mechanism. Additionally, a Na^{+} ion was identified as bound with five main-chain carbonyl oxygens in three out of four molecules in the asymmetric unit (Figure 2D). Many nucleases require two metal ions for complete enzymatic activity (40), but a Na^{+} ion has no known role in the enzymatic activity of ZC3H12C or other family members. The PIN domain also exhibited a positively charged region covering the extended antiparallel β-sheet (β4/β5), revealing a potential RNA-binding platform (Figure 2B).

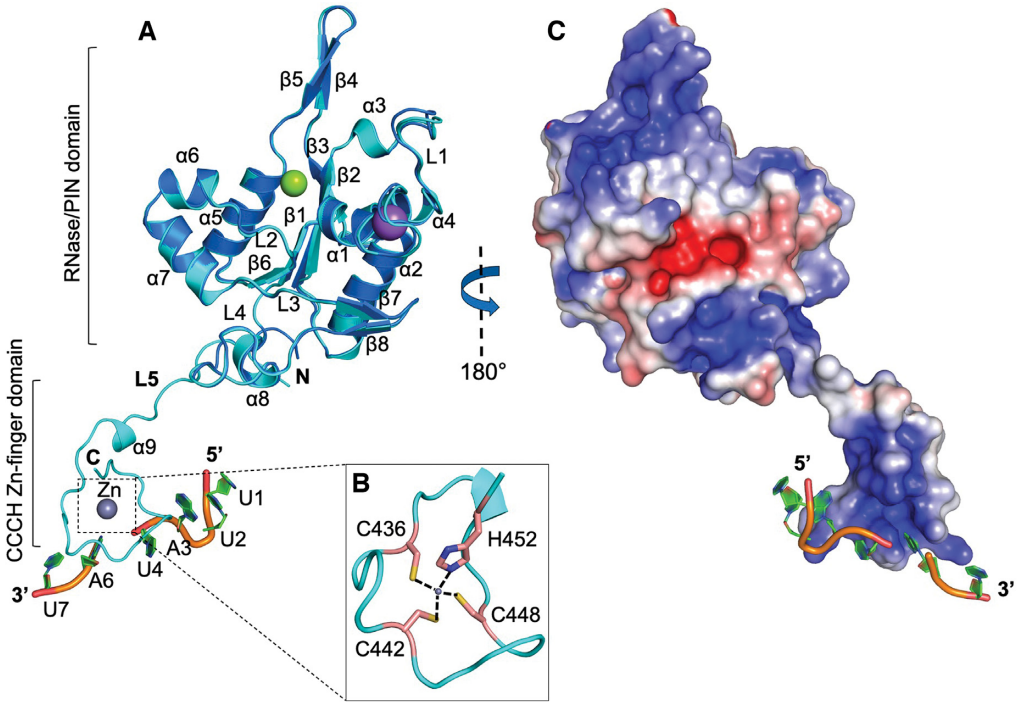

Figure 3. Crystal structure of *Mm*ZC3H12C-RNA complex. (**A**) Cartoon representation of PIN-Zf-r(UUAUUAU) complex structure (cyan) superimposed with the Mg^{2+} (green sphere) bound apo N-PIN structure (blue). The PIN domain adopts a Rossmann-like α/β/α sandwich fold and is linked with the CCCH ZnF-RNA complex via linker L5. The RNA oligonucleotide is cleaved at rU5, presumably due to the residual RNase activity of the crystallized protein (see Figure 1E). The ZnF is complete with a bound Zn^{2+} ion (gray sphere), which is (**B**) coordinated between the Cys436, Cys442, Cys448 and His452 residues from the ZFD. (**C**) The electrostatic surface of PIN-Zf oriented at 180° to the cartoon view. The PIN domain is polar and exhibits a positively charged patch close to the catalytic Mg^{2+} ion. A positively charged deep groove is visible across the ZFD surface, which is involved in stacking interactions with RNA. The electrostatic surface potential is displayed with a range from –5 (red) to +5 kT/e (blue).

Crystal structure of ZC3H12C–RNA complex

To investigate the structural basis of ZC3H12C mediated RNA targeting, we further co-crystallized *Mm*ZC3H12C_PIN-$Zf^{(260–458)}$ D271N with an RNA heptamer, r(UUAUUAU), an A/U rich element of similar sequence to the RNA fragment binding to Tis11d CCCH ZnF (19). The crystals belonged to space group $P4_1$ and accommodated two protein molecules in one asymmetric unit with one polypeptide chain (molecule-1) exhibiting electron density for the PIN domain only. However, in the second chain (molecule-2), the PIN domain was connected with the ZFD, and a RNA oligonucleotide could be traced in the electron density.

The PIN domain structure in the complex is remarkably similar to the apo PIN structure with an RMSD of ∼0.3 Å suggesting that RNA binding proceeds without structural changes of the protein (Figure 3A). The ZC3H12C ZnF is one of the shortest CCCH-type zinc fingers with a consensus sequence $C^1X_5C^2X_5C^3X_3H$ and adopts a compact globular fold with a Zn^{2+} ion bound between the conserved Cys436, Cys442, Cys448 and His452 side chains (Figure 3B). The ZFD is linked with the PIN domain via linker L5 and exhibits a positively charged deep groove running across its surface, facilitating the stacking of different RNA bases (Figure 3C). Due to the residual RNase activity of the crystallized protein (Figure 1E, lane2), RNA substrate is apparently cleaved at rU5 and the electron density for all but rU5 is observed in the structure (Figure S3B, D). Notably, the linker L5 is completely structured and adopts an extended conformation, thus positioning the ZFD away from the PIN domain.

Although the ZFD is distant from the PIN domain, analysis of the crystal packing revealed two possible modes (mode-I and mode-II) of ZnF-RNA complex docking onto the neighboring PIN domain (molecule-1), revealing crucial interactions between RNA and PIN domain (Figure S3A). In mode-I, the ZnF tucks the 5′ terminal rU1 base into the positively charged pocket on the PIN domain surface (Figure S3B), resulting in hydrogen bond formation between rU1 O2′ and Arg330 and between rU1 O4 and Arg344. The rU2 and rA3 bases are stabilized via hydrogen bonds linking OP1 with Arg330 and Lys447, respectively (Figure S3C). Mode-I clearly suggests that the PIN domain directly interacts with RNA via surface-exposed basic residues. A significant reduction in RNA targeting by both Lys314Ala and Arg330Ala mutation confirm their involvement in RNA interaction *in vitro* (Figure 4C) and *in vivo* (Figure 4D). A similar effect on RNA targeting was previously observed for the Arg214 residue in ZC3H12A (30), the structural equivalent of ZC3H12C Arg344.

In mode-II, however, the ZnF brings the RNA strand close to the catalytic site of the PIN domain (Figure S3A,D) and facilitates hydrogen bonding between rU1 O4 and Asn375 from the L2 loop. The rU2 base directly interacts with Asn375, while rA3 N6 and N7 are linked with

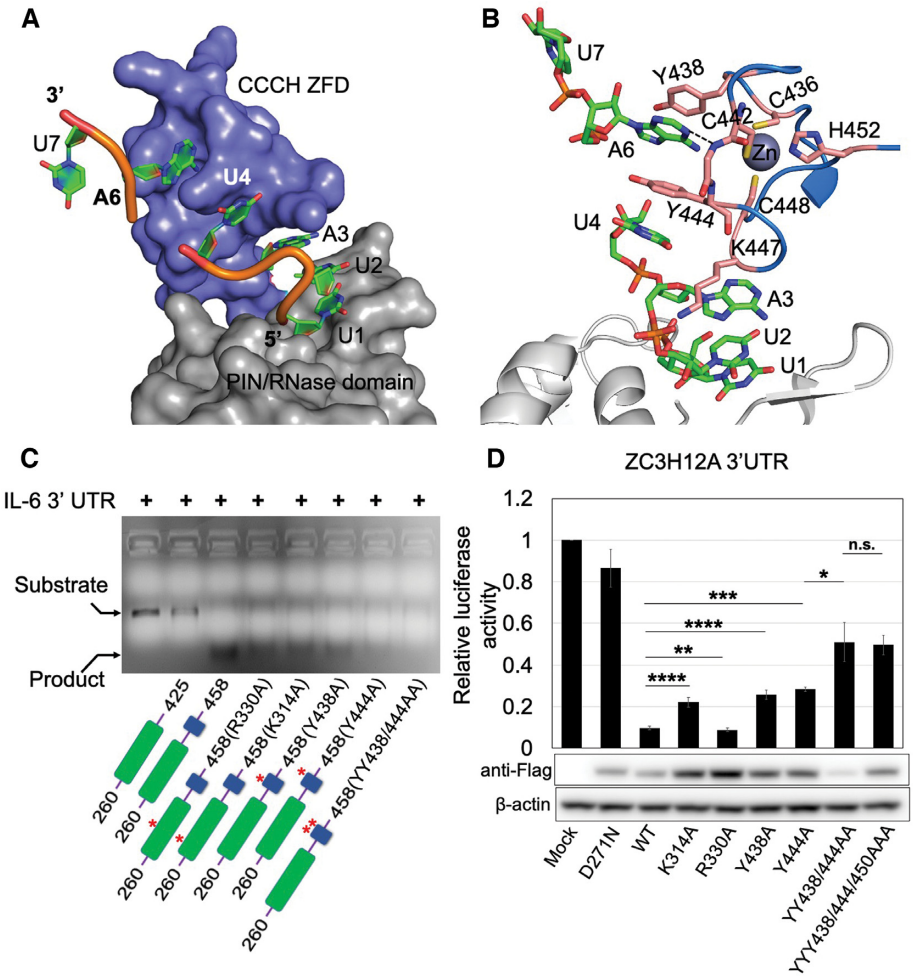

Figure 4. ZC3H12C PIN-CCCH ZnF mediated RNA interaction. (**A**) Surface representation of the PIN-ZFD fragment demonstrating the interactions with the RNA heptanucleotide (shown as cartoon) in mode-I. The rU1 nucleotide is docked onto the PIN domain (gray), while rU4 and rA6 are stacked into a hydrophobic pocket on the ZnF surface. The rA3 base is docked under the surface-exposed K447 side chain from the ZFD. (**B**) Molecular interactions between RNA and ZnF showing that the U4 and A6 bases (green sticks) are stabilized via base stacking against the conserved Y444, Y438 and Y444 (orange) residues. (**C**) Denaturing agarose gel showing the effect of different point mutations on RNA degradation by ZC3H12C. PIN domain mutants R330A, K314A and, ZFD Y438A, Y444A and YY/AA double mutant exhibit less product formation as compared to WT PIN-Zf$^{(260–458)}$ demonstrating reduced RNase activity due to defects in RNA recognition. The PIN and ZFD are shown in green and blue respectively, with the mutations labeled in the domain diagrams. (**D**) Luciferase reporter assay demonstrating the RNase activity of the *Mm*ZC3H12C_FL mutants against ZC3H12A 3′UTR. Both Tyr438 and Tyr444 mutants show significantly reduced RNase activity compared to WT. Lys314 and Arg330, also show significantly reduced RNase activity when mutated, confirming their involvement in RNA binding *in vivo*. The Western blot of the cell lysate used in the luciferase assay shows the expression level of different ZC3H12C mutants. The expression level of mutant proteins was generally higher than that of native ZC3H12C. The luciferase data are presented as mean ± SD ($n = 3$). *$P < 0.05$; **$P < 0.01$; ***$P < 0.001$; ****$P < 0.0001$ (two-tailed Student's *t*-test). n.s., not significant.

Asp374 via two water-mediated hydrogen bonds (Figure S3E). Asp374 is one of the catalytic residues, and a mutation to Ala or Asn results in decreased catalytic activity in ZC3H12A (30,41). Upon RNA binding, there is only a subtle conformational change in Asp374 implicating that it might not be directly involved in catalysis but rather in substrate binding, and the reduced catalytic activity of the mutant might be due to defects in RNA binding.

The nucleotides rU4 and rA6 are inserted into a hydrophobic pocket on the ZnF surface (Figure 4A) and stabilized via base stacking interactions with the surface exposed Tyr444 and Tyr438, respectively. An additional hydrogen bond between rA6 N1 and the Thr441 amide further stabilizes the stacking (Figure 4B). However, the rU7 nucleotide fails to interact with any protein residue and remains mostly solvent-exposed, with only few interactions with a water molecule *via* its Watson-Crick edge. The stacking interactions have been known to be crucial in RNA recognition by CCCH ZnFs (19–21,42–44), and our CCCH ZnF structure demonstrates that such short ZnF not only adopts a globular fold, but also puts these evolutionarily conserved interactions to use in RNA recognition. Because we were never able to observe the ZnF in structures of apo ZC3H12C, it remains difficult to comment on structural changes in the ZnF that may be induced upon RNA binding. The two interaction modes described above are clearly supported by structural and biochemical data, but it is not yet possible to

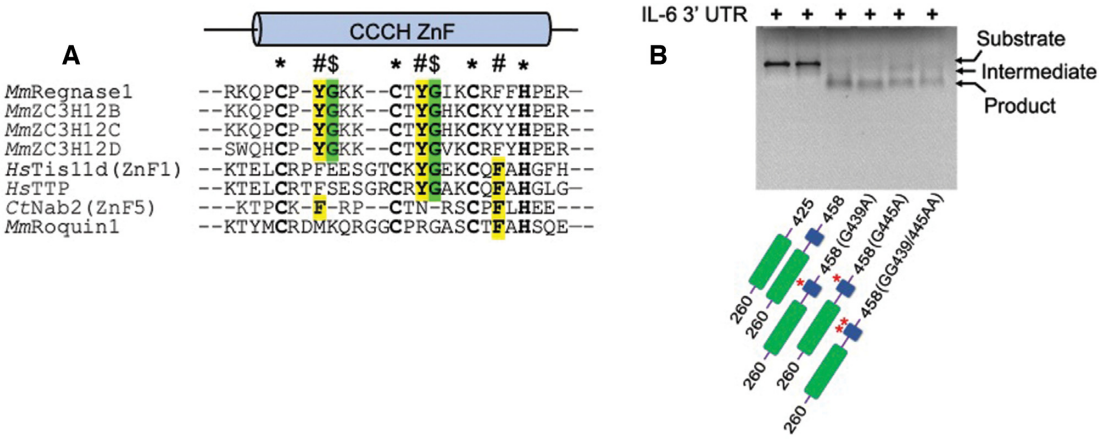

Figure 5. (**A**) Comparative sequence alignment of the CCCH ZnF of ZC3H12/Regnase members with other characterized CCCH type ZnFs (Tis11d, TTP, Nab2 and Roquin1). The CCCH ZnF in all four ZC3H12 family members is highly conserved and exhibits two tyrosine residues (highlighted in yellow) involved in RNA base stacking. Two glycine residues (green) are also conserved in ZC3H12 family proteins, facilitating a sharp backbone bend, and only Tis11d family members contain one such glycine residue. Conserved RNA-interacting aromatic residues in other CCCH ZnFs are also highlighted in yellow. (**B**) Denaturing agarose gel showing the effect of glycine mutations on IL-6–3′UTR degradation by ZC3H12C. These glycines adopt a unique backbone conformation, and the G439A, G445A and GG/AA double mutants (shown at the gel bottom) exhibit significantly reduced RNase activity as compared to WT PIN-Zf$^{(260–458)}$ and form less product RNA, resulting from a crippled ZFD. The PIN and ZFD are shown in green and blue color respectively, with glycine mutations also shown in the domain diagrams.

decide which of these mutually exclusive modes is relevant for the biological function of ZC3H12C.

Unique ZC3H12 ZnF mediated RNA recognition

Next, we examined if Tyr438 and Tyr444 mediated base stacking is crucial in RNA degradation and compared the RNase activity of PIN-Zf$^{(260–458)}$ Tyr/Ala mutants with WT protein by analyzing the amount of product RNA liberated in an *in vitro* RNase assay. Different ZC3H12C variants degraded the IL-6–3′UTR_WT RNA into an intermediate and product RNA with the PIN-Zf$^{(260–458)}$ (WT) generating maximum product. By comparison, Y438A and Y444A single mutants generated significantly less RNA cleavage product, while a Y438A/Y444A double mutation led to further reduction in product formation, implicating a reduced RNase activity (Figure 4C). Since the Tyr438 and Tyr444 side chains are involved in stacking of one (rU4) and two (rU4 and rA6) nucleobases, respectively, the observed difference in the RNase activity of these two mutants is also explained. Besides that, a cell-based luciferase assay also showed reduced RNase activity of ZC3H12C Tyr/Ala mutants confirming that Tyr mediated base stacking is crucial in RNA targeting by ZC3H12C. However, the third aromatic residue from the ZC3H12C ZnF (Tyr450) is dispensable, because a YYY438/444/450AAA triple mutant does not exhibit further significant reduction in RNA targeting as compared to the YY438/444AA double mutant (Figure 4D). Since the ZFD is highly conserved in the entire ZC3H12 family, an identical mode of RNA recognition by the ZFD in other members is very likely.

We also identified two conserved glycines (Gly439 and Gly445) next to the RNA interacting tyrosine residues in the ZC3H12 ZnFs (Figure 5A). These glycine residues adopt a unique backbone conformation, which facilitates a compact ZnF fold. We examined their importance by comparing the RNase activity of ZnF Gly/Ala mutants with WT protein by analyzing the product RNA liberated after 15 min incubation. As expected, the ZC3H12C G439A, G445A and GG439/445AA mutants generated significantly less product RNA compared to WT (Figure 5B), confirming that, indeed, the observed ZnF fold requires the glycine residues′ unique conformation which appears crucial for efficient RNA targeting. Surprisingly, in a 5 min incubation reaction the G439A mutant yielded more product RNA than WT ZC3H12C (Figure S4), which further indicates that the unique backbone conformation induced by Gly439 keeps the ZC3H12C RNase activity checked, most likely by limiting interactions of Tyr438 with specific RNA motifs. However, a Gly439 mutation may enhance the structural flexibility of the neighboring Tyr438, probably allowing this side chain to interact with non-specific RNA motifs, thus explaining the higher catalytic activity.

DISCUSSION

ZC3H12/Regnase family members are CCCH-type ZnF containing RNases, which play crucial roles in immune response regulation by post-transcriptional targeting of inflammatory cytokine mRNA (45). Despite several studies on ZC3H12A/Regnase-1, crucial structural information on how target RNA is recognized by the ZC3H12 proteins remained elusive. In this study, we present the first crystal structures of the ZC3H12C PIN domain with and without the unique CCCH-type ZnF domain and an RNA heptanucleotide which, together with systematic biochemical analysis, reveal unprecedented insight in RNA recognition by ZC3H12 family proteins.

Our *in vitro* biochemical experiments confirm that ZC3H12C is an active ribonuclease which requires both its PIN domain and ZFD for full catalytic activity (Figure 1A-D), strongly implicating a cooperative RNA bind-

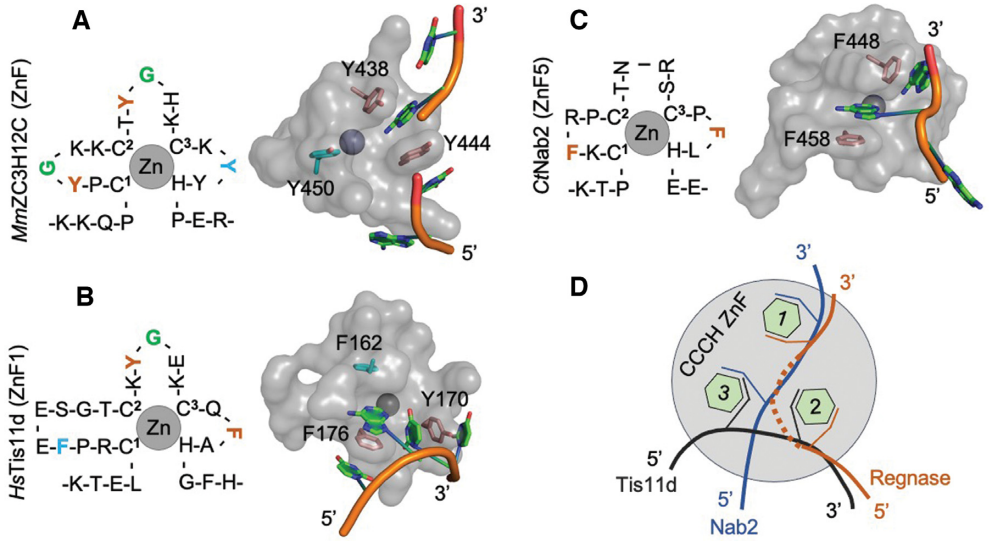

Figure 6. Unique structural features of the ZC3H12C CCCH ZnF in RNA recognition. Schematic and tertiary structures of (**A**) *Mm*ZC3H12C ZnF, (**B**) *Hs*Tis11d (ZnF1) and (**C**) *Ct*Nab2 (ZnF5) are shown with substrate RNA immobilized on the ZnF scaffolds via base stacking with just two aromatic residues. These aromatic residues (bold orange) are conserved in the C^2-X_n-C^3/C^3-X_n-H motif in *Hs*Tis11d and the C^1-X_n-C^2/C^3-X_n-H motif in *Ct*Nab2, while ZC3H12C ZnF is structurally unique in utilizing Y438 and Y444 from the C^1-X_5-C^2 and C^2-X_5-C^3 motifs for RNA binding. The third aromatic residue (cyan) in ZC3H12C ZnF (Y450) and Tis11d (F162) is dispensable in RNA binding. The conserved glycines in the ZC3H12C (G439, G445) and Tis11d (G171) ZnFs, which bend the Cα backbone by adopting a unique Gly-dependent conformation are also highlighted (green) in the schematic structure. These glycines are absent in Nab2, which, however, depends on more than two ZnFs in tandem for efficient RNA binding. (**D**) Simplified model of RNA alignment on the CCCH ZnF surface via spatially conserved aromatic residues (shown as green hexagons) from different ZnFs. Combination of two out of three residues facilitates specific RNA substrates to dock in unique orientation onto the ZnF scaffolds. The aromatic residues form a bent groove on the ZC3H12C ZnF surface. Although the RNA is cleaved (shown as dotted golden line), this implies a unique orientation with significantly bent RNA backbone as compared with RNA in Tis11d (black) and Nab2 (blue) ZnFs.

ing by both domains. Notably, the mutated ZC3H12C construct PIN-Zf$^{(260–458)}$ D271N, but not the N-PIN-Zf$^{(177–458)}$ D271N catalytic mutant shows a minimal *in vitro* RNase activity (Figure 1E), suggesting that the N-motif of ZC3H12C (aa 177–260) might be involved in regulation of its RNase activity. This observation is supported by an NMR study of ZC3H12A, which suggests regulation of RNase activity by direct interaction between N-motif and PIN domain (41). The interacting residues between PIN and N-motif are conserved in ZC3H12A and ZC3H12C proteins, suggesting a direct interaction between PIN and N-motif. Nevertheless, a crystal structure of substrate RNA-bound ZC3H12C would be required to prove that the N-motif modulates RNase activity. ZC3H12C displays Mg^{2+} ion dependent catalytic activity, which is strongly supported by the presence of a bound Mg^{2+} ion in the PIN domain structure (N-PIN$^{(177–425)}$) (see Figure 2A). In addition, we show that ZC3H12C exhibits catalytic activity against an IL-6 3′UTR RNA sequence and requires its N-PIN-Zf-C$^{(177–474)}$ element for a controlled activity against target RNA.

In crystal structures of the ZC3H12C PIN domain, more than one molecule is present in the asymmetric unit of the crystal, however, SEC (see Figure 1C) and RALS experiments (data not shown) for different variants confirm a monomeric nature in solution. Although the ZC3H12A PIN domain has been suggested to adopt a dimeric arrangement, our RALS and size exclusion analysis (data not shown) indicated only monomers in solution. In addition to these observations, two specific aspects of RNA degradation by ZC3H12C require particular attention.

The ZC3H12C ZnF exhibits unique structural features for RNA recognition, conserved in the whole ZC3H12 family

ZC3H12 proteins harbor one of the shortest CCCH-type zinc fingers in the human proteome with consensus motif $C^1X_5C^2X_5C^3X_3H$ (18), and present unique structural features in RNA recognition among CCCH ZnF-family proteins. Our structural analysis reveals that RNA recognition in CCCH ZnFs is dictated by three conserved aromatic residues (Figure 4), each present in the C^1-X_n-C^2, C^2-X_n-C^3 and C^3-X_n-H motif, respectively (Figures 5A and 6A). Out of four CCCH ZnF–RNA complex structures known to date, *Hs*Tis11d utilizes aromatic residues in the C^2-X_n-C^3 and C^3-X_n-H motifs (Figure 6B) (19), while yeast Nab2 requires aromatic residues from its C^1-X_n-C^2 and C^3-X_n-H motifs for RNA stacking (Figure 6C) (20,21). Interestingly, the ZC3H12 CCCH ZnF utilizes aromatic residues in the C^1-X_5-C^2 and C^2-X_5-C^3 motifs (Figure 6A), thereby aligning RNA in a unique orientation on the ZnF scaffold (Figure 6D). Besides that, only a single aromatic residue from the C^3-X_n-H motif is crucial in *Mm*Unkempt (43) and *Mm*MBNL1 (44) mediated RNA stacking, however, its structural equivalent in C^3-X_n-H motifs of ZC3H12 ZnF is not accessible for RNA interaction and hence dispensable as also observed in the luciferase assay.

Another novel feature of the ZC3H12 ZnF is the presence of two unique glycines (Gly439, Gly445) in the center of the C^1-X_5-C^2 and C^2-X_5-C^3 motifs, which bend the Cα backbone by adopting a unique conformation, disfavored

for other amino acids (46), thus facilitating a compact functional ZnF fold (Figures 5A and 6A). The *Hs*Tis11d family ZnFs contain only one such conserved glycine in the C^2-X_n-C^3 motif (Figure 6B) (19), while such glycine residues are absent in C^3-X_n-H motifs in the entire CCCH-ZnF protein family.

The 3D structural superimposition of all characterized CCCH-type ZnFs revealed that the RNA interacting aromatic residues are spatially conserved, and a variety of RNA substrates are specifically recognized by different CCCH ZnF proteins, simply by utilizing unique combinations of conserved aromatic residues (Figure 6D). This observation not only suggests a divergent evolution of CCCH ZnF proteins from a common ancestor, but also explains the involvement of these proteins in a multitude of biological functions including immune responses, neuronal differentiation, alternative splicing, polyadenylation and mRNA decay (6,15,18,43,44,47) by post-transcriptional targeting of different mRNAs.

ZC3H12 CCCH-ZnF mediated RNA trinucleotide recognition

The crystal structure of a ZC3H12C PIN ZnF-RNA complex reveals that the D271N mutant, for which we found residual RNase activity *in vitro*, represents a post-catalytic state as the RNA is cleaved at rU5, generating a rU4 3′OH group through Mg^{2+} dependent catalysis. ZC3H12A was also shown to generate product RNA with 3′OH termini *in vitro* (17,41) suggesting a conserved catalytic mechanism in the ZC3H12 ribonuclease family. Since no electron density for rU5 is observed, it is difficult to conclude if it is completely excised or simply fails to dock onto the ZnF surface.

CCCH ZnFs are known to recognize 2 to 3 ribonucleotides per ZnF (20,43), and our structure of ZC3H12C's unique CCCH ZnF exhibits features of recognizing a RNA trinucleotide sequence as well. The crystallized ZnF-RNA complex reveals a positively charged groove running across the ZFD surface with U4 and A6 bases stacked into the groove. Additionally, a positively charged empty groove is available between the rU4 and rA6 binding pockets, which might represent a binding site for the missing rU5 on the ZFD surface. To support this observation, we superimposed the ZC3H12C ZnF-RNA complex atop a *Hs*Tis11d ZnF1-RNA complex (PDB 1rgo) (19), which clearly shows that a pyrimidine (rU) base bound by Tis11d perfectly occupies the position equivalent to the missing rU5 in the empty groove of ZC3H12C without any clashes (Figure 7A). The central rU5 would form multiple hydrogen bonds with the Lys449 amino group and the Zn^{2+} ion coordinating Cys436 and Cys448 via its Watson–Crick edge (Figure 7B), which, together with the stacked flanking nucleotides (5′ rU4 and 3′ rA6), would favor a bend in the RNA backbone, likely representing a loop region of a stem–loop structure. Since the ZFD is highly conserved in the entire ZC3H12 protein family, for future research it will be crucial to delineate the differences in RNA targeting between the four ZC3H12 RNases, which likely target a similar RNA stem-loop structure.

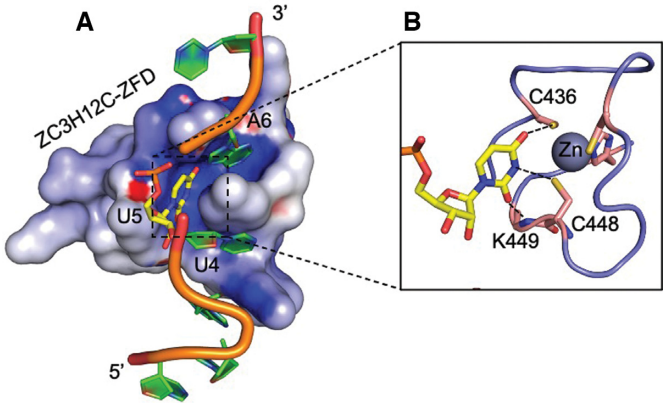

Figure 7. The ZC3H12C ZnF harbors a binding platform for RNA trinucleotide recognition. (**A**) Electrostatic surface representation of ZC3H12C ZnF-RNA together with a pyrimidine nucleotide (rU3) from the superimposed *Hs*Tis11d (ZnF1)-r(UA**U**U) structure. The superimposed nucleotide occupies the empty groove on the ZnF surface, demonstrating a tri-nucleotide recognition by the ZnF. The ZC3H12C RNA is shown as cartoon, while the added pyrimidine (yellow) is shown as sticks. (**B**) Molecular interactions of the superimposed uridine with the ZC3H12C ZnF (shown as cartoon). The aligned uridine would form hydrogen bonds (shown as dotted lines) with K449, C436 and C448 residues from the ZFD via its Watson-Crick edge.

DATA AVAILABILITY

The atomic coordinates and structure factors have been deposited in the Protein Data Bank under accession codes 7ndi for ZC3H12C N-$PIN^{(177–425)}$, 7ndh for PIN-$Zf^{(260–458)}$, 7ndk for the $PIN^{(260–425)}$ D271 catalytic mutant and 7ndj for the PIN–$Zf^{(260–458)}$–RNA complex.

SUPPLEMENTARY DATA

Supplementary Data are available at NAR Online.

ACKNOWLEDGEMENTS

We acknowledge the beamline support by the staff of Helmholtz-Zentrum Berlin für Materialien und Energie at BESSY, Berlin. We highly acknowledge Prof. Leemor Joshua-Tor for allowing to perform revision experiments in her research lab at Cold Spring Harbor Laboratory. U.H. and A.G. conceived and coordinated the study. A.G. performed the experiments and Y.R. assisted with diffraction data acquisition and structure analysis. S.Y. and T.U. performed the luciferase assays for ZnF mutants. A.G. analyzed the data and wrote the manuscript, which was further revised by U.H. and O.T..

FUNDING

Max-Delbrück Center for Molecular Medicine in the Helmholtz Association, Berlin, Germany. Funding for open access charge: Max Delbrück Centre for Molecular Medicine, Berlin.

Conflict of interest statement. None declared.

REFERENCES

1. Carpenter,S., Ricci,E.P., Mercier,B.C., Moore,M.J. and Fitzgerald,K.A. (2014) Post-transcriptional regulation of gene expression in innate immunity. *Nat. Rev. Immunol.*, **14**, 361–376.
2. Schwanhausser,B., Busse,D., Li,N., Dittmar,G., Schuchhardt,J., Wolf,J., Chen,W. and Selbach,M. (2011) Global quantification of mammalian gene expression control. *Nature*, **473**, 337–342.
3. Castello,A., Fischer,B., Eichelbaum,K., Horos,R., Beckmann,B.M., Strein,C., Davey,N.E., Humphreys,D.T., Preiss,T., Steinmetz,L.M. *et al.* (2012) Insights into RNA biology from an atlas of mammalian mRNA-binding proteins. *Cell*, **149**, 1393–1406.
4. Castello,A., Fischer,B., Frese,C.K., Horos,R., Alleaume,A.M., Foehr,S., Curk,T., Krijgsveld,J. and Hentze,M.W. (2016) Comprehensive identification of RNA-binding domains in human cells. *Mol. Cell*, **63**, 696–710.
5. Gerstberger,S., Hafner,M. and Tuschl,T. (2014) A census of human RNA-binding proteins. *Nat. Rev. Genet.*, **15**, 829–845.
6. Liang,J., Wang,J., Azfer,A., Song,W., Tromp,G., Kolattukudy,P.E. and Fu,M. (2008) A novel CCCH-zinc finger protein family regulates proinflammatory activation of macrophages. *J. Biol. Chem.*, **283**, 6337–6346.
7. Liang,J., Song,W., Tromp,G., Kolattukudy,P.E. and Fu,M. (2008) Genome-wide survey and expression profiling of CCCH-zinc finger family reveals a functional module in macrophage activation. *PLoS One*, **3**, e2880.
8. Matsushita,K., Takeuchi,O., Standley,D.M., Kumagai,Y., Kawagoe,T., Miyake,T., Satoh,T., Kato,H., Tsujimura,T., Nakamura,H. *et al.* (2009) Zc3h12a is an RNase essential for controlling immune responses by regulating mRNA decay. *Nature*, **458**, 1185–1190.
9. Tsoi,L.C., Spain,S.L., Knight,J., Ellinghaus,E., Stuart,P.E., Capon,F., Ding,J., Li,Y., Tejasvi,T., Gudjonsson,J.E. *et al.* (2012) Identification of 15 new psoriasis susceptibility loci highlights the role of innate immunity. *Nat. Genet.*, **44**, 1341–1348.
10. Munir,S., ber Rahman,S., Rehman,S., Saba,N., Ahmad,W., Nilsson,S., Mazhar,K. and Naluai,A.T. (2015) Association analysis of GWAS and candidate gene loci in a Pakistani population with psoriasis. *Mol. Immunol.*, **64**, 190–194.
11. Von Gamm,M., Schaub,A., Jones,A. N., Wolf,C., Behrens,G., Lichti,J., Essig,K., Macht,A., Pircher,J., Ehrlich,A. *et al.* (2019) Immune homeostasis and regulation of the interferon pathway require myeloid-derived Regnase-3. *J. Exp. Med.*, **216**, 1700–1723.
12. Liu,L., Zhou,Z., Huang,S., Guo,Y., Fan,Y., Zhang,J., Zhang,J., Fu,M. and Chen,Y.E. (2013) Zc3h12c inhibits vascular inflammation by repressing NF-κB activation and pro-inflammatory gene expression in endothelial cells. *Biochem. J.*, **451**, 55–60.
13. Mizgalska,D., Wegrzyn,P., Murzyn,K., Kasza,A., Koj,A., Jura,J., Jarzab,B. and Jura,J. (2009) Interleukin-1-inducible MCPIP protein has structural and functional properties of RNase and participates in degradation of IL-1beta mRNA. *FEBS J.*, **276**, 7386–7399.
14. Dobosz,E., Wilamowski,M., Lech,M., Bugara,B., Jura,J., Potempa,J. and Koziel,J. (2016) MCPIP-1, alias Regnase-1, controls epithelial inflammation by posttranscriptional regulation of IL-8 production. *J. Innate Immun*, **8**, 564–578.
15. Mino,T., Murakawa,Y., Fukao,A., Vandenbon,A., Wessels,H.H., Ori,D., Uehata,T., Tartey,S., Akira,S., Suzuki,Y. *et al.* (2015) Regnase-1 and Roquin regulate a common element in inflammatory mRNAs by spatiotemporally distinct mechanisms. *Cell*, **161**, 1058–1073.
16. Iwasaki,H., Takeuchi,O., Teraguchi,S., Matsushita,K., Uehata,T., Kuniyoshi,K., Satoh,T., Saitoh,T., Matsushita,M., Standley,D.M. *et al.* (2011) The IκB kinase complex regulates the stability of cytokine-encoding mRNA induced by TLR-IL-1R by controlling degradation of regnase-1. *Nat. Immunol.*, **12**, 1167–1175.
17. Wilamowski,M., Gorecki,A., Dziedzicka-Wasylewska,M. and Jura,J. (2018) Substrate specificity of human MCPIP1 endoribonuclease. *Sci. Rep.*, **8**, 7381.
18. Fu,M. and Blackshear,P.J. (2017) RNA-binding proteins in immune regulation: a focus on CCCH zinc finger proteins. *Nat. Rev. Immunol.*, **17**, 130–143.
19. Hudson,B.P., Martinez-Yamout,M. A., Dyson,H. J. and Wright,P. E. (2004) Recognition of the mRNA AU-rich element by the zinc finger domain of TIS11d. *Nat. Struct. Mol. Biol.*, **11**, 257–264.
20. Kuhlmann,S.I., Valkov,E. and Stewart,M. (2014) Structural basis for the molecular recognition of polyadenosine RNA by Nab2 Zn fingers. *Nucleic Acids Res.*, **42**, 672–680.
21. Brockmann,C., Soucek,S., Kuhlmann,S.I., Mills-Lujan,K., Kelly,S.M., Yang,J.C., Iglesias,N., Stutz,F., Corbett,A.H., Neuhaus,D. *et al.* (2012) Structural basis for polyadenosine-RNA binding by Nab2 Zn fingers and its function in mRNA nuclear export. *Structure*, **20**, 1007–1018.
22. Schlundt,A., Heinz,G.A., Janowski,R., Geerlof,A., Stehle,R., Heissmeyer,V., Niessing,D. and Sattler,M. (2014) Structural basis for RNA recognition in roquin-mediated post-transcriptional gene regulation. *Nat. Struct. Mol. Biol.*, **21**, 671–678.
23. Leppek,K., Schott,J., Reitter,S., Poetz,F., Hammond,M.C. and Stoecklin,G. (2013) Roquin promotes constitutive mRNA decay via a conserved class of stem-loop recognition motifs. *Cell*, **153**, 869–881.
24. Schuetz,A., Murakawa,Y., Rosenbaum,E., Landthaler,M. and Heinemann,U. (2014) Roquin binding to target mRNAs involves a winged helix-turn-helix motif. *Nat. Commun.*, **5**, 5701.
25. Garg,A. and Heinemann,U. (2017) A novel form of RNA double helix based on G·U and C·A+ wobble base pairing. *RNA*, **24**, 209–218.
26. Scheich,C., Kummel,D., Soumailakakis,D., Heinemann,U. and Bussow,K. (2007) Vectors for co-expression of an unrestricted number of proteins. *Nucleic Acids Res.*, **35**, e43.
27. Mueller,U., Darowski,N., Fuchs,M.R., Forster,R., Hellmig,M., Paithankar,K.S., Puhringer,S., Steffien,M., Zocher,G. and Weiss,M.S. (2012) Facilities for macromolecular crystallography at the Helmholtz-Zentrum Berlin. *J. Synchrotron Radiat.*, **19**, 442–449.
28. Krug,M., Weiss,M. S., Heinemann,U. and Mueller,U. (2012) XDSAPP: a graphical user interface for the convenient processing of diffraction data using XDS. *J. Appl. Crystallogr.*, **45**, 568–572.
29. McCoy,A.J., Grosse-Kunstleve,R.W., Storoni,L.C. and Read,R.J. (2005) Likelihood-enhanced fast translation functions. *Acta Crystallogr. D. Biol. Crystallogr.*, **61**, 458–464.
30. Xu,J., Peng,W., Sun,Y., Wang,X., Xu,Y., Li,X., Gao,G. and Rao,Z. (2012) Structural study of MCPIP1 N-terminal conserved domain reveals a PIN-like RNase. *Nucleic Acids Res.*, **40**, 6957–6965.
31. Adams,P.D., Afonine,P.V., Bunkoczi,G., Chen,V.B., Davis,I.W., Echols,N., Headd,J.J., Hung,L.W., Kapral,G.J., Grosse-Kunstleve,R.W. *et al.* (2010) PHENIX: a comprehensive Python-based system for macromolecular structure solution. *Acta Crystallogr. D. Biol. Crystallogr.*, **66**, 213–221.
32. Emsley,P., Lohkamp,B., Scott,W.G. and Cowtan,K. (2010) Features and development of Coot. *Acta Crystallogr. D. Biol. Crystallogr.*, **66**, 486–501.
33. Murshudov,G.N., Vagin,A. A. and Dodson,E. J. (1997) Refinement of macromolecular structures by the maximum-likelihood method. *Acta Crystallogr. D. Biol. Crystallogr.*, **53**, 240–255.
34. Painter,J. and Merritt,E.A. (2006) Optimal description of a protein structure in terms of multiple groups undergoing TLS motion. *Acta Crystallogr. D. Biol. Crystallogr.*, **62**, 439–450.
35. Chen,V.B., Arendall,W.B 3rd, Headd,J.J., Keedy,D.A., Immormino,R.M., Kapral,G.J., Murray,L.W., Richardson,J.S. and Richardson,D.C. (2010) MolProbity: all-atom structure validation for macromolecular crystallography. *Acta Crystallogr. D. Biol. Crystallogr.*, **66**, 12–21.
36. Davis,I.W., Leaver-Fay,A., Chen,V.B., Block,J.N., Kapral,G.J., Wang,X., Murray,L.W., Arendall,W.B. 3rd, Snoeyink,J., Richardson,J.S. *et al.* (2007) MolProbity: all-atom contacts and structure validation for proteins and nucleic acids. *Nucleic Acids Res.*, **35**, W375–W383.
37. Baker,N.A., Sept,D., Joseph,S., Holst,M.J. and McCammon,J.A. (2001) Electrostatics of nanosystems: application to microtubules and the ribosome. *Proc. Natl. Acad. Sci. U.S.A.*, **98**, 10037–10041.
38. Holm,L. and Rosenstrom,P. (2010) Dali server: conservation mapping in 3D. *Nucleic Acids Res.*, **38**, W545–W549.
39. Ceska,T.A., Sayers,J.R., Stier,G. and Suck,D. (1996) A helical arch allowing single-stranded DNA to thread through T5 5′-exonuclease. *Nature*, **382**, 90–93.
40. Yang,W. (2011) Nucleases: diversity of structure, function and mechanism. *Q. Rev. Biophys.*, **44**, 1–93.
41. Yokogawa,M., Tsushima,T., Noda,N.N., Kumeta,H., Enokizono,Y., Yamashita,K., Standley,D.M., Takeuchi,O., Akira,S. and Inagaki,F.

(2016) Structural basis for the regulation of enzymatic activity of Regnase-1 by domain-domain interactions. *Sci. Rep.*, **6**, 22324.
42. Lai,W.S., Perera,L., Hicks,S.N. and Blackshear,P.J. (2014) Mutational and structural analysis of the tandem zinc finger domain of tristetraproline. *J. Biol. Chem.*, **289**, 565–580.
43. Murn,J., Teplova,M., Zarnack,K., Shi,Y. and Patel,D.J. (2016) Recognition of distinct RNA motifs by the clustered CCCH zinc fingers of neuronal protein Unkempt. *Nat. Struct. Mol. Biol.*, **23**, 16–23.
44. Teplova,M. and Patel,D.J. (2008) Structural insights into RNA recognition by the alternative-splicing regulator muscleblind-like MBNL1. *Nat. Struct. Mol. Biol.*, **15**, 1343–1351.
45. Takeuchi,O. (2018) Endonuclease Regnase-1/Monocyte chemotactic protein-1-induced protein-1 (MCPIP1) in controlling immune responses and beyond. *Wiley Interdiscip. Rev. RNA*, **9**, e1449.
46. Lovell,S.C., Davis,I.W., Arendall,W.B. 3rd, de Bakker,P.I., Word,J.M., Prisant,M.G., Richardson,J.S. and Richardson,D.C. (2003) Structure validation by Cα geometry: φ,ψ and Cβ deviation. *Proteins*, **50**, 437–450.
47. Maeda,K. and Akira,S. (2017) Regulation of mRNA stability by CCCH-type zinc-finger proteins in immune cells. *Int. Immunol.*, **29**, 149–155.